Effect of acetylcholine deficiency on neural oscillation in a brainstem-thalamus-cortex model related with Alzheimer's disease

Hao Yang
Shaanxi Normal University
XiaoLi Yang (yangxiaoli@snnu.edu.cn)
Shaanxi Normal University
SiLu Yan
Shaanxi Normal University
ZhongKui Sun
Northwestern Polytechnical University

Article

Keywords: Alzheimer's disease, acetylcholine deficiency, power spectrum, amplitude distribution, neural mass model

Posted Date: June 6th, 2022

DOI: https://doi.org/10.21203/rs.3.rs-1648878/v1

Effect of acetylcholine deficiency on neural oscillation in a brainstem-thalamus-cortex model related with Alzheimer's disease

Hao Yang[1], XiaoLi Yang[*1], SiLu Yan[1], ZhongKui Sun[2]
[1]School of Mathematics and Statistics, Shaanxi Normal University, Xi'an 710062, PR China
[2] School of Mathematics and Statistics, Northwestern Polytechnical University, Xi'an 710072, PR China

Abstract

Previous works imply that involving brainstem in neuropathological studies of Alzheimer's disease (AD) is of clinically significant. Abnormality of cholinergic system also underlies the neurodegeneration during AD. This work constructs a comprehensive neural mass model for cholinergic neuropathogenesis that involves brainstem, thalamus and cortex, wherein how acetylcholine deficiency in AD affects neural oscillation of the model output is systematically explored from the perspective of neurocomputation. By decreasing synapse connectivity parameters in direct cholinergic pathway from brainstem to thalamus and indirect glutamatergic synapse pathway from cortex to brainstem to mimic the pathological condition of reduced acetylcholine release in patients with AD, the property of neural oscillation in this model is numerically investigated by means of power spectrum in frequency domain and amplitude distribution in time domain. Simulated results demonstrate that decreasing synapse connectivity whether in the direct cholinergic pathway or the indirect glutamatergic synapse pathway can alter the neural oscillation significantly in three aspects: it induces an obvious decrease of dominant frequency; it leads to a degraded rhythmic activity in alpha frequency band as well as an enhanced rhythmic activity in theta frequency band; it results in reduced oscillation amplitude of the model output. These results are agreement with the characteristic of electrophysiological EEG measurement recorded in AD, especially support the hypothesis that cholinergic deficiency is a promising pathophysiological origin of EEG slowing in AD. Our analysis indicates that targeting the cholinergic system may have potential prospects in early diagnosis and treatment of AD.

[*] Corresponding author.
Email address: yangxiaoli@snnu.edu.cn (XiaoLi Yang).

Key words: Alzheimer's disease, acetylcholine deficiency, power spectrum, amplitude distribution, neural mass model

1. Introduction

As we all know, the brain is the largest and most complex structure of the central nervous system, which is closely related to consciousness, language, memory and other activities [1]. Damage to some brain regions would cause neurological or psychiatric disorders such as epilepsy, Alzheimer's disease (AD) and autism. AD is a neurodegenerative disease of the nervous system in the elderly. Only when irreversible damage occurs to the brain can AD be detected, so it poses a very serious threat to the health of AD patients [2].

The cholinergic hypothesis indicates that the cholinergic system in patients with AD is abnormal. Cholinergic action is important to maintain attention and memory [3 4]. Relevant studies have found that there are massive loss of cholinergic neurons and decrease of acetylcholine releases in the brain of AD patients [5 6 7 8]. In addition, the brainstem contains a large number of cholinergic neurons projecting to the thalamus [9 10 11] which can maintain the cortical excitability during wakefulness and rapid eye movement sleep [12 13]. In order to check the brainstem nuclei have vulnerability to AD-related pathological changes, Parvizi et al. [14] have performed a study of thioflavin S-stained serial sections in the entire brainstem, in which they have found that the physiological markers of AD, senile plaques and neurofibrillary tangles, are respectively existed in superior colliculus and cholinergic nucleus in 32 patients with AD, whereas no changes are seen in the brainstem of 26 normal subjects. The above findings imply that AD may relate with the degeneration of cholinergic neurons in the brainstem, especially the cholinergic pathway from the brainstem to the thalamus may be important to understand the pathogenesis of AD.

There are considerable laboratory researches, such as neuroimaging, neurochemistry and gene mapping, to identify potential AD marker for early preventative treatments of AD. Electroencephalographic (EEG), for its sensitivity to underlying brain pathology, relative non-invasiveness and ease of measurement, has become a popular neurophysiological technique to study AD. Some typical EEG changes including the reduced dominant frequency (also called peak frequency) [15 16 17] and the slowing of EEG signals in AD patients [17 18 19 20 21] have been revealed. Moreover, in a review of EEG dynamics in AD patients, Jeong [20] has stated that the pathophysiological origin for EEG slowing in AD may be largely due to acetylcholine deficiency. This statement is also supported by EEG experiment in

healthy subjects using scopolamine (a kind of muscarinic receptor antagonist), in which there appears an increase in delta and theta power and a decrease in alpha and beta power after administrating scopolamine [22].

In order to better understand the mechanism behind the activity of brain neurons, many neurocomputational models have been developed, roughly categorized as detailed model and neural mass model [23 24 25 26 27 28 29]. In the former of detailed model, the neural dynamics is described at the level of individual neurons by incorporating the kinetics of synaptic channels explicitly [29]. This kind of model is helpful to understand the basic mechanism of neural dynamics at a microscopic scale, whereas it is too computationally complicated to analyze the whole behavior in a relatively large brain region. In the latter of neural mass model, each cell population represents a neuronal ensemble of mesoscopic scale, which is lumped together and supposed to share same membrane potential. Thus, the dynamics of the entire populations together with their synapse are described just by several differential equations. Each population performs two mathematical operations in these neural mass models [28]. One is that the average membrane potential in each population receiving from all afferent neuronal populations is changed into an average density of spikes, which is usually simulated by a sigmoidal function. The other one is that each population sends synapses to other populations, which converts the presynaptic spike density into the postsynaptic membrane potential by a second linear transform function of pulse response with different parameters. One of the first neural mass model is proposed first by Wilson and Cowan [30 31] based on the interaction of one excitatory population and one inhibitory population. Then, Silva et al. [32] have established an alpha rhythm model in the thalamus to mimic the generation of the alpha rhyth. Subsequently, Jansen and Rit [33] have changed the impulse response function to construct a neural mass model containing pyramidal neuron population, excitatory interneuron population and inhibitory interneuron population in a single cortical column. Wendling et al. [34] have included the population of GABA interneurons with fast synaptic kinetics into the Jason and Rit model, where they produce realistic mutichannel epileptiform EEG signal in the hippocampus during the transition from interictal to fast ictal activity. Nowadays, the neural mass model proposed by Jansen and Rit has been frequently extended to coupled neural mass models to simulate the complexity of EEG dynamics in large cortical region [28 29 34 35 36]. In addition, Bhattacharya et al. have proposed a thalamus-cortex-thalamus (TCT) neural mass model consisting of a thalamic module and a cortical module, in

which the synaptic connectivity related to the aberration of alpha rhythm in the brain resulting from AD is discussed [37]. Recently, Li et al. have improved the TCT model by incorporating the disinhibition property between different inhibitory interneurons in the cortical region and introducing the full relay function of thalamus to the cortical region [26]. This work is helpful to understand the neuronal correlates of alpha rhythm slowing as a result of AD.

Although some neural mass models comprising cortical column, thalamus or hippocampus have been successfully exploited to simulate some specific aspects of brain rhythms and the abnormal brain activity during disease, they have not been used to analyze the underlying brain dynamics in the brainstem associated with AD. In addition, as indicted in the previous work [9 12 14], in brainstem there are different nuclei involving in many functions, such as controlling homeostasis and emotions, modulating the cognitive functions of cerebral cortex, thus understanding its involvement in AD is clinically significant. Nevertheless, the status of most subcortical structures including the brainstem remains poorly understood during AD compared with the majority of neuropathological studies of AD from the cortical aspect. Some manifestations of AD (e.g. behavioral, affective, and cognitive abnormality) may be interpreted from the perspective of dysfunction in subcortical structure of brainstem [14]. Thus, this work extends the neural mass model to build a comprehensive model in the interactive brain structures of brainstem, thalamus and cortex (i.e., a BTC model) with a purpose to mimic the EEG dynamics observed in patients of AD, therein explore how abnormal acetylcholine release influences neural oscillation of the model output.

The following is organized as follows. Firstly, model presentations including how to construct the BTC model and its related model parameters are illustrated in Section 2. Then the effect of reduced synapse connectivity resulting from AD on the neural oscillation in this BTC model is systematically studied by numerical simulations in Section 3. Finally, a brief summary of this work is present.

2. An enhanced neural mass model: brainstem-thalamus-cortex model

As described in the Introduction, in addition to the thalamic and cortical aspects, the involvement of brainstem is also of significance to AD [9 12 14]. In this section, based on the visual pathway, a comprehensive neural mass model in the interactive brain regions of brainstem, thalamus and cortex (BTC) is firstly constructed. As

shown in Fig 1, this BTC model is made of a brainstem module, a thalamus module and a cortex module. There are two populations of superior colliculus (SC) and pedunculopontine nucleus (PNN) in the brainstem module, inside which the PNN population produces excitatory synapse on the SC population as implied by the work [11]. The thalamus module is modeled by three populations of thalamic relay nucleus (TRC), inhibitory interneurons (IN), thalamic reticular nucleus (TRN) [26 32 37 38 39]. The TRC population receives inhibitory inputs from the IN and TRN populations via intrinsic synapse pathway, whereas the TRN population receives excitatory inputs from the TRC population. The IN and TRN populations also receive inhibitory inputs from themselves, respectively. The module of cortex is built upon four populations of pyramidal neurons(PY), excitatory interneurons (eIN), fast inhibitory interneurons (fIN) and slow inhibitory interneurons (sIN) [26 28 29 34 37]. Within this module, the PY population sends excitatory outputs to the sIN and fIN populations, in turn, both the sIN and fIN populations send inhibitory outputs to the PY population. There are reciprocal excitatory outputs between the PY and eIN populations, and there are reciprocal inhibitory outputs between the sIN and fIN populations. For the interconnections between the three modules, as indicated in the studies [9 10 11 40 41] there are cholinergic and glutamatergic synapse pathway from the brainstem area to the thalamus area. The thalamic nuclei are modulated by an ascending cholinergic projection from the brainstem via cholinergic neurotransmitter. Depending on different muscarinic receptor subtypes, the PNN population sends exhibitory outputs to the TRC population by means of M1 and M3 receptor subtypes [42], also it sends inhibitory outputs to the IN and TRN populations by means of M2 receptor subtype [9 10 11 43]. Meanwhile, the SC population in the brainstem sends excitatory outputs to the TRC and IN populations via glutamatergic neurotransmitter [40 41]. The synaptic interconnections between the thalamus and the cortex modules conform to the classical results as presented in the literatures [26 36 37], i.e., all the populations of TRC, IN and TRN in the thalamus region receive excitatory inputs from the PY population, on the same time, the TRC population sends excitatory outputs to all the populations of PY, eIN, fIN and sIN in the cortical region. Beside the ascending synapses from the brainstem to the thalamus and cortex, there is also important descending synapse pathway from the cortex to the brainstem in the central nervous system [44 45]. Here, the PY population in the cortex module sends excitatory inputs to the SC and PNN populations in the brainstem module. The other extrinsic sources to the BTC model come from the retinal and nearby cortical formations, i.e., the

retinal population sends excitatory inputs to the IN, TRC and SC populations, and the PY population receives excitatory afferent from nearby cortical regions [26 28 29 36 37].

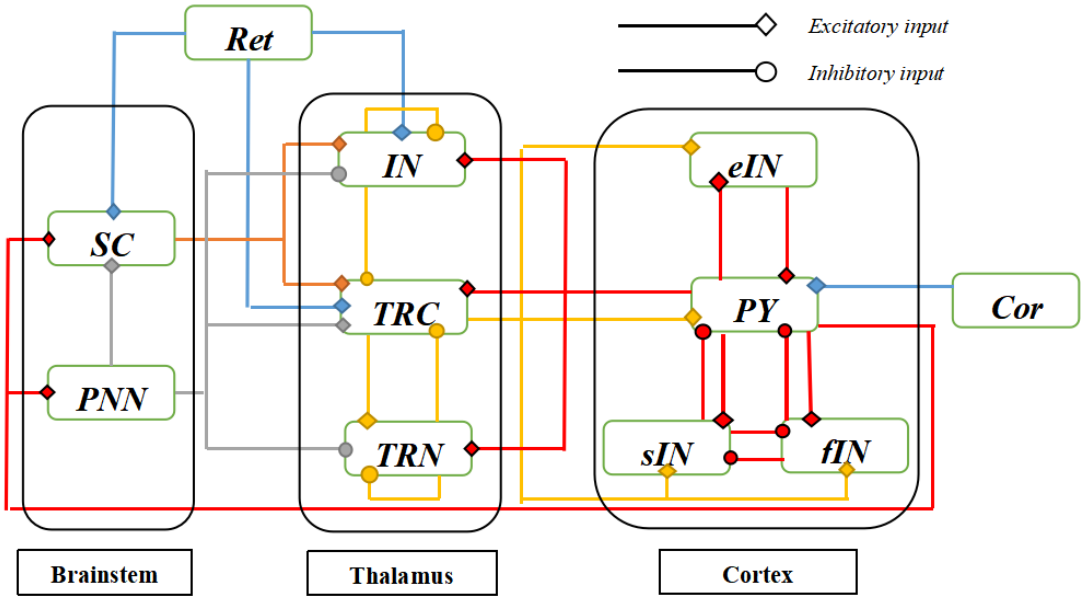

Fig 1 The layout for module structure and synaptic connectivity in the BTC model. The BTC model comprises of three formations: brainstem module, thalamus module and cortex module. In the brainstem module there are two populations of superior colliculus (SC) and pedunculopontine nucleus (PNN). In the thalamus module there are thalamic relay nucleus (TRC), inhibitory interneurons (IN) and thalamic reticular nucleus (TRN). In the cortex module there are pyramidal neurons(PY), excitatory interneurons (eIN), fast inhibitory interneurons (fIN) and slow inhibitory interneurons (sIN). Ret and Cor denote external visual inputs and adjacent cortical inputs respectively. Diamond represents excitatory inputs and circle represents inhibitory inputs.

For convenience, neuron populations in this model are denoted by different lowercase letters s, d, i, t, n, x, p, f, l, r and c, which represent population SC, PNN, IN, TRC, TRN, eIN, PY, fIN, sIN, Ret, Cor, respectively. According to the technique of neural mass model, the kinetic equations governing each population is obtained by performing two mathematical operations. One is that the average membrane potential in each population a (here $a = s, d, i, t, n, x, p, f, l, r, c$) receiving from all afferent neuronal populations is changed into an average density of spikes , which is usually simulated by the following sigmoidal

function:

$$\varphi_a = S(V_a) = \frac{2e_0}{1+e^{\sigma(V_0-V_a)}} \tag{1}$$

$$V_a = \sum_b C_{abe} x_b - \sum_d C_{adi} x_d \tag{2}$$

where C_{abe} represents excitatory synaptic connection parameters between postsynaptic neuron population a and presynaptic neuron population b, C_{adi} represents inhibitory synaptic connection parameters between postsynaptic neuron population a and presynaptic neuron population d, x_a, x_b and x_d is postsynaptic potential (PSP) respectively generated by population a, b and d. e_0 determines the maximum firing rate, V_0 is the firing threshold, σ controls the steepness of this sigmoid function. Here the standard values are set as $e_0 = 2.5s^{-1}$, $V_0 = 6mV$, $\sigma = 0.56mV^{-1}$ sourced from Jansen and Rit's work [33]. Note that the average density of spike for neuron population Ret is simulated by Gaussian white noise with mean μ_1 and variance φ_1. The average density of spike for neuron population Cor is simulated by Gaussian white noise with mean μ_2 and variance φ_2. In the following, the parameters for the Gaussian white noise are set as $\mu_1 = 11$, $\varphi_1 = 2$, $\mu_2 = 30$ and $\varphi_2 = 2$ [37].

The other one is that a second linear transform function of pulse response converts the presynaptic spike density into the postsynaptic membrane potential, which is as follows:

$$\tau_a^2 x_a'' = A_a \tau_a \varphi_a - 2\tau_a x_a' - x_a \tag{3}$$

where A_a is the synaptic strength determining the maximum amplitude of PSP, and τ_a represents the time constant of PSP.

The connectivity parameters of afferent to the brainstem and thalamus modules are according to the previous physiological data [46 47 48 49 50]. In detail, based on the electron microscopic observances on the connectivity patterns of two main cell types

in the lateral geniculate nucleus of the cat, Erisir et al. [46] have revealed that distribution of synapse is different between relay cells and interneurons present in this nucleus. The relative distribution of terminal types contacting relay cells is $14.6 \pm 0.6\%$ retinal (RLP) terminals, $29.6 \pm 1.6\%$ inhibitory (F) terminals, and $55.8 \pm 1.7\%$ cortex and brainstem terminals. Whereas, the analysis of the total synaptic inputs onto the interneurons indicates that interneurons receive $37.8 \pm 1.0\%$ of all synapses from retinal terminals, $26.8 \pm 1.5\%$ from inhibitory terminals, and $35.4 \pm 1.8\%$ from cortex and brainstem terminals. Moreover, in geniculate A-laminae the relay cells and the interneurons receive 85.8 ± 0.6 % and $14.2 \pm 0.6\%$ of all synaptic terminals combined, respectively, i.e., the synaptic terminals contacting the relay cells is about 6 times of that contacting the interneurons. Erisir et al. [47] have further found that the relative number of cortical inputs and brainstem inputs to the lateral geniculate nucleus is of the same order, each of whose terminals constitutes roughly one-half. As for the TRN afferent axons, Jones have reported that almost 70% synaptic afferent to the reticular nucleus in the somatosensory sector of the rat reticular nucleus are attributed to corticothalamic terminals, 20-25% are attributed to thalamocortical collateral synapses, 15-20% are attributed to $GABA_{ergic}$ synapses and a quite small number of afferent are from the brainstem [48]. Another study has reported that the synaptic proportions from corticothalamic, thalamocortical and $GABA_{ergic}$ synapse are respectively 60-65%, 20% and 15% [49]. On the basis of the above studies [46 47 48 49 50] the connectivity parameters relative with the brainstem and thalamus modules are set as $C_{sre}=8.5$, $C_{sde}=8$, $C_{spe}=20$, $C_{dpe}=60$, $C_{tre}=48.2$, $C_{tii}=48.8$, $C_{tni}=48.8$, $C_{tpe}=92$, $C_{tde}=92$, $C_{tse}=50$, $C_{ire}=20.8$, $C_{iii}=14.7$, $C_{ipe}=9.7$, $C_{ise}=30$, $C_{idi}=9.7$, $C_{nte}=11$, $C_{nni}=8.3$, $C_{npe}=30.3$, $C_{ndi}=5.5$. The connectivity parameters afferent to the cortex module are sourced from the works [26 28 33 34 51], i.e., $C_{pce}=1$, $C_{pte}=80$, $C_{pxe}=108$, $C_{pli}=33.75$, $C_{pfi}=108$, $C_{xte}=100$, $C_{xpe}=135$, $C_{lte}=40$, $C_{lpe}=33.75$, $C_{lfi}=13.5$, $C_{fte}=40$, $C_{fpe}=40.5$, $C_{fli}=13.5$. On the same time, the synaptic strength and time constant in the BTC model are chosen as follows: the synaptic strength A_a for PNN, SC, TRC, PY, eIN, IN, TRN, sIN and fIN is respectively 5.2, 2.4, 3.25, 2.7, 2.7, 22, 22, 4.5 and 39mv; the time constant τ_a for

PNN, SC, TRC, PY, eIN, IN,TRN, sIN and fIN respectively 1/160, 1/80, 1/100, 1/40, 1/40, 1/40, 1/40, 1/20 and 1/300 s.

3. Main Result

As described in the Introduction, previous reports about reduced ACh releases, loss of cholinergic neurons and decreased ChAT activity in AD patients have indicated that acetylcholine release is abnormal in AD patients [5 6 7 8]. In brainstem there are a large amount of cholinergic neurons projecting to thalamus, moreover, the brainstem nuclei such as superior colliculus and cholinergic nucleus are susceptible to AD [9 10 11]. This implies that AD is associated with degeneration of the direct cholinergic pathway from brainstem to thalamus. In addition, the neuroimaging technique has showed that cortical areas losing functional/structural connectivity from graph theoretical studies have been related to cortical atrophy in AD [52 53]. This property of cortical atrophy may influence the descending synapse projection from cortex to brainstem [44 45], which in turn could weaken the cholinergic pathway from brainstem to thalamus indirectly. Thus, this study simulates the pathological condition of reduced acetylcholine release in AD by decreasing the synapse connectivity parameters in the direct cholinergic pathway from brainstem to thalamus (i.e., C_{tde} from PNN to TRC, C_{idi} from PNN to IN, C_{ndi} from PNN to TRN) and the indirect glutamatergic synapse pathway from cortex to brainstem(i.e., C_{dpe} from PY to PNN). How the abnormal acetylcholine release affects neural oscillation in this BTC model is systematically explored by means of power spectrum and amplitude distribution.

In the following, the second-order differential equations governing the BTC model are numerically solved by Euler method in an environment of MATLAB 2019a. The total simulation time is 120s with a time resolution of 1/256s. The model output corresponds to the summated postsynaptic potential V_{trc} in the TRC population. For each output vector, an epoch is extracted in the interval of [20,120] s to ensure that all the transients are discarded. The epoch of output is then bandpass filtered by a Butterworth filter of order 10 with a lower and upper cut-off frequencies of 0.5 and 50 Hz respectively. The detailed analysis of power spectrum and oscillation amplitude are further carried out based on the filtered output.

3.1 Decreasing the excitatory cholinergic connectivity from PNN to TRC

The level of cholinergic neurotransmitter from the PNN population in the brainstem module to the TRC population in the thalamus module is determined by the excitatory synapse connectivity parameter C_{tde}. In this section, through decreasing the strength C_{tde} to mimic the degeneration of acetylcholine release in patients with AD, neural oscillation of this BTC model is firstly characterized by means of power spectrum analysis in frequency-domain. Based on the filtered output of V_{trc}, the power spectrum density of the BTC model is computed using the Welch technique with a Hamming window. Quantitative analysis of power spectrum is performed by characterizing dominant frequency and measuring relative power in specific frequency bands. Dominant frequency is a frequency captured at which the power spectrum density reaches its peak. The relative power of alpha band(8-13Hz) or theta band(4-8Hz) is calculated by averaging the relative power spectrum density within the corresponding frequency band.

The dominant frequency of the model output is illustrated in **Fig 2** when the connectivity parameter C_{tde} is varied in the rage of [60,100]. On the whole, the dominant frequency shows a downward trend upon decreasing C_{tde} from 100 to 60: it is initially within alpha band, then the dominant frequency decreases steadily until C_{tde} is decreased to a critical value of about 80, at which the dominant frequency transits from alpha band to theta band, afterwards it decreases continually within theta band as C_{tde} is further decreased. That is to say, the smaller the excitatory cholinergic synapse connectivity parameter C_{tde}, the lower the dominant frequency. This phenomenon is further vividly confirmed by some individual plots of power spectrum density. **Fig 3** depicts the detailed power spectrum density when the connectivity C_{tde} is successively chosen as 100, 82, 70 and 60. Clearly, peaks of the power spectrum density in the upper two panels are concentrated at the alpha frequency band of 9.25 and 8.5 respectively when C_{tde} is more than 80, whereas peaks in the lower two panels are centered at the theta frequency band of 7 and 6 respectively when C_{tde} is less than 80. These interesting results indicate that acetylcholine deficiency, a biomarker for AD, can induce an obvious decrease of dominant frequency, which is

consistent with the electrophysiological experiment results that the dominant/peak frequency of EEG is significantly lower in early stage of AD than control subjects [15 16 17].

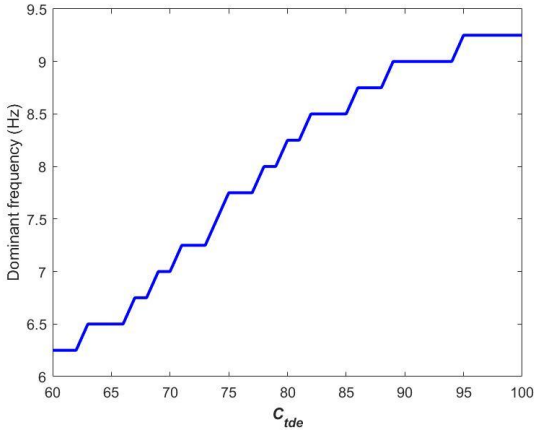

Fig 2 Dependence of the dominant frequency of the BTC model output on the excitatory cholinergic synapse connectivity C_{tde} from PNN to TRC.

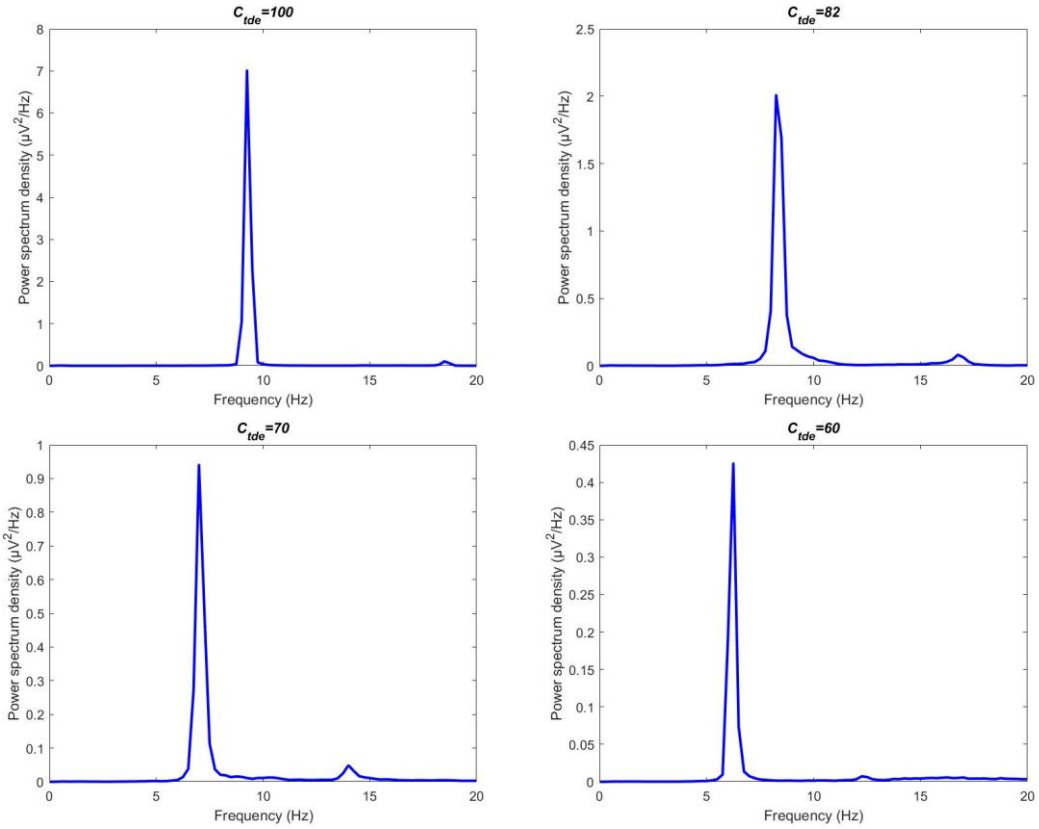

Fig 3 The individual plots of power spectrum density when the excitatory cholinergic synapse connectivity parameter C_{tde} takes some different values of 100, 82, 70 and 60.

Furthermore, the power spectrum analysis of relative power in specific frequency bands are carried out. The relative power within alpha band and within theta band is respectively illustrated in **Fig 4** when the excitatory synapse connectivity parameter C_{tde} is in the range of [60,100]. One can observe that upon decreasing C_{tde} from 100 the relative alpha band power decreases slightly until C_{tde} arrives at the critical value of about 80, then it falls sharply till $C_{tde} \approx 73$, after which the relative power in alpha band does not decrease anymore and basically tends to be stable. Interestingly, the evolution of the relative theta band power is opposite to that of the relative alpha band power. In detail, upon decreasing C_{tde} from 100 to 60, the relative power in theta band is just a little increased till C_{tde} reaches the critical value of about 80, then it grows swiftly until $C_{tde} \approx 73$, after that the relative theta band power fluctuates slightly with the further decrease of C_{tde}. This phenomenon accords with the traditional experiment EEG measurements that there are a decrease in alpha band activity and an increase in theta band activity in patients with AD [17 18 19 20 21], in particular, it supports the hypothesis that cholinergic deficiency is a promising pathophysiological origin of the EEG slowing in AD [20 22].

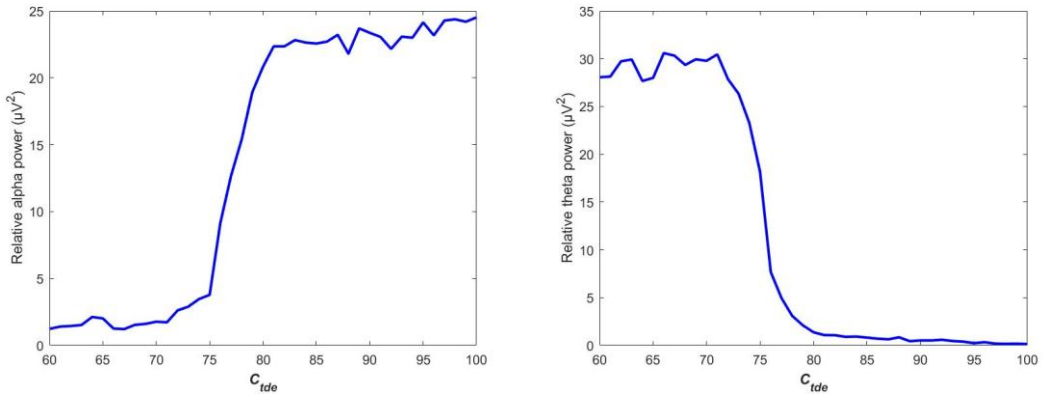

Fig 4 The evolution of relative power in specific frequency bands during the excitatory synapse connectivity parameter C_{tde} is varied in the range of [60,100]: (left) the relative power within alpha band, (right) the relative power within theta band.

Secondly, neural oscillation of this BTC model is investigated by means of oscillation amplitude in time-domain. When decreasing the excitatory synapse connectivity parameter C_{tde} from 100 to 60, the model output, i.e., the summated

postsynaptic potential V_{trc} in the TRC population, is illustrated in **Fig 5** for each value of C_{tde}. The longitudinal coordinate (y-axis) of this figure is the summated postsynaptic potential V_{trc} during [20, 120] s of simulations. Obviously, as a whole the oscillation amplitude of V_{trc} is getting smaller upon decreasing the synapse connectivity parameters C_{tde}. To visualize this result, the postsynaptic potential V_{trc} for some typical synaptic strengths such as C_{tde}= 60, 70, 82, and 100 is also depicted in **Fig 6**. From the left panels one can qualitatively observe that the oscillation amplitude of V_{trc} is gradually reduced with the decrease of connectivity parameter. Especially, for the two former ones the BTC model produces rhythmic oscillation of potential analogous to alpha-rhythm (with the dominant frequency within alpha band as shown in **Fig 3**), i.e., they exhibit waxes and wanes in amplitude just like a form of spindle [32]. There is no obvious qualitative change in dynamics from the perspective of time series. As the synapse connectivity C_{tde} is less than the critical value of 80, the output of BTC model in the latter two panels presents rhythmic oscillation of theta frequency band (with the dominant frequency within theta band as shown in **Fig 3**) with relative small amplitude compared to the former two cases. Furthermore, as displayed in the right panels the statistical property of oscillatory potential is characterized by amplitude distribution based on 500 realizations of postsynaptic potential. Here the histogram of oscillation amplitude is fitted by normal density function with estimated parameters of mean and variance. As can be seen in the right panels, the estimated mean of oscillation amplitude is 11.04, 8.68, 5.87 and 3.43 when the connectivity parameter C_{tde} is successively taken as 100, 82, 70 and 60. This result further quantitively confirms that the reduced oscillation amplitude of the model output results from the decreased excitatory synapse connectivity parameter C_{tde}, a hallmark of deficit cholinergic synapse pathway from the PNN population to the TRC population.

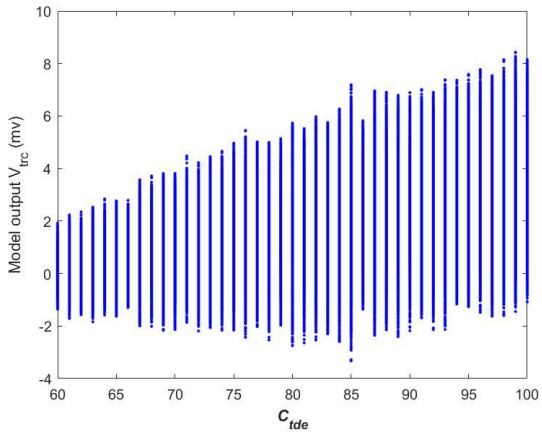

Fig 5 The model output of the summated postsynaptic potential V_{trc} for each excitatory synapse connectivity parameter C_{tde} in the range of [60,100].

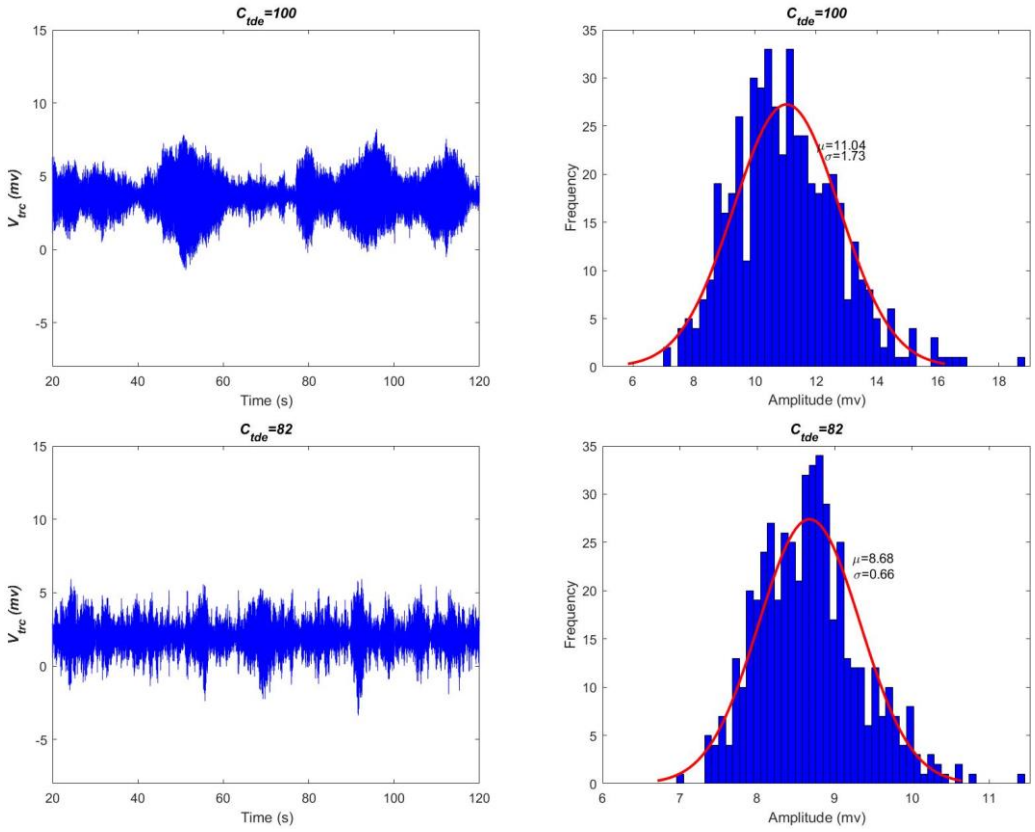

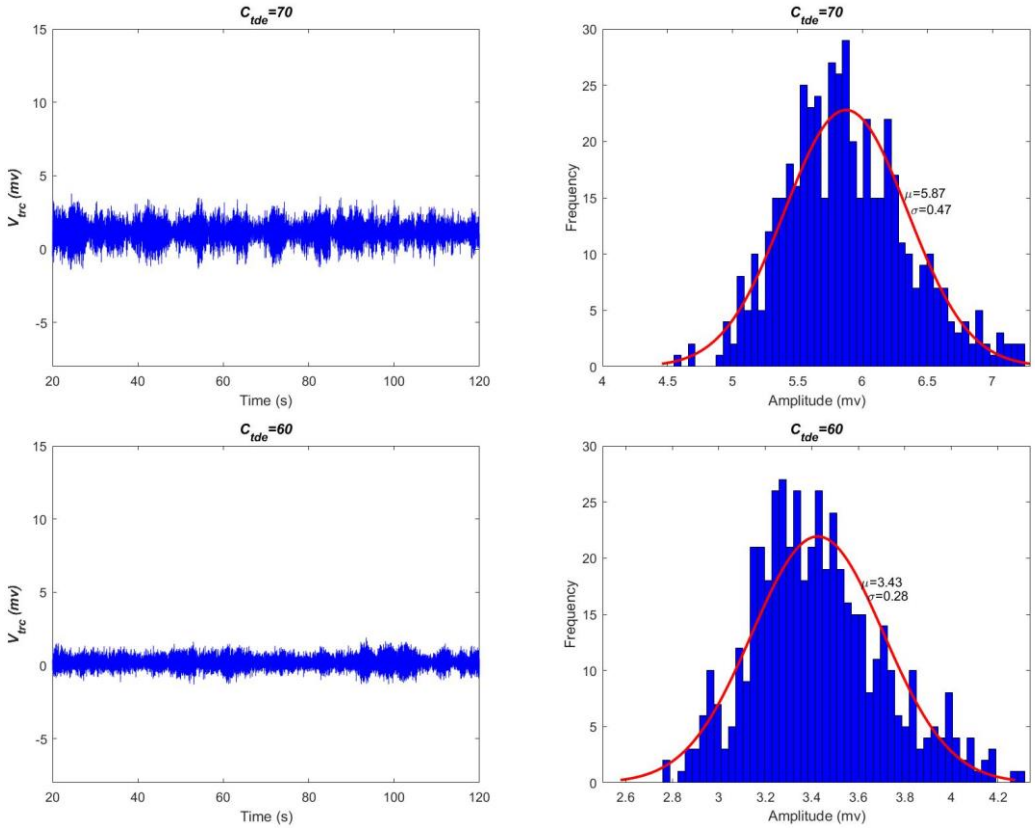

Fig 6 Plots of the summated postsynaptic potential V_{trc} (left panels) and the corresponding amplitude distribution of V_{trc} (right panels) for some different connectivity parameter values. From top to bottom, the connectivity parameter C_{tde} is in turn 100, 82, 70 and 60.

3.2 Decreasing the inhibitory cholinergic connectivity from PNN to IN and TRN

In addition to the above excitatory cholinergic pathway from PNN to TRC via M1 and M3 muscarinic receptor subtypes, there are also two inhibitory cholinergic pathways from PNN to IN and TRN via M2 muscarinic receptor subtype, whose synaptic connection are determined by C_{idi} and C_{ndi}, respectively. In this section, the physiological feature of acetylcholine deficiency in AD patients is reflected by reducing C_{idi} or C_{ndi}. Under such environment, the neural oscillation in the BTC model is investigated by means of power spectrum in frequency-domain and amplitude distribution in time-domain.

Firstly, neural oscillation of this BTC model is discussed on the basis of power spectrum analysis. The variation of dominant frequency of the model output V_{trc} with the decrease of inhibitory cholinergic synaptic strength is delineated in **Fig 7**. One can

see that whether decreasing the synapse connectivity parameter C_{idi} (from PNN to IN) or C_{ndi} (from PNN to TRN), they can always lead to a decrease of dominant frequency. To be specific, when C_{idi} (or C_{ndi}) is decreased from 18 (or 10) to a critical value of about 5 (or 2), the dominant frequency gradually drops within alpha band, then it steps into theta band and continually drops within theta band. To illustrate above result more detail, some power spectrum density curves are exhibited in **Fig 8** for different synaptic connectivity parameter values. In the left column, C_{idi} is taken as 10, 6, 3 and 1 from top to bottom. Clearly, when C_{idi} is greater than 5, the frequency corresponding to the maximum of power spectrum density is respectively at 9.25 and 8.25, whereas when C_{idi} is less than 5, the frequency corresponding to the maximum of power spectrum density is respectively at 7 and 6. That is to say, the dominant frequency for the upper two figures and the bottom two figures is within alpha band and theta band respectively. In the right column, C_{ndi} is taken as 7, 3, 1.5 and 0.5 from top to bottom. Obviously, when C_{ndi} is larger than 2, the dominant frequency in the upper two panels is at the alpha frequency band of 9.25 and 8.5 respectively, yet the dominant frequency in the lower two panels is at the theta frequency band of 7.5 and 7.25 respectively when C_{ndi} is smaller than 2. In addition, the relative power of the model output is calculated with the change of inhibitory cholinergic synapse connectivity C_{idi} and C_{ndi} in **Fig 9**. The relative theta and alpha band power is denoted by the red and blue curves, respectively. From the two panels, we can observe that upon decreasing synapse connectivity the relative theta band power increases mildly until C_{idi} (or C_{ndi}) reaches the critical value of about 5 (or 2), then it increases sharply with the further decrease of synapse connectivity. Interestingly, the relative alpha band power decreases slowly till C_{idi} (or C_{ndi}) reaches the critical value of about 5 (or 2), after that it decreases swiftly with a further reduction of synapse connectivity.

In a word, the reduction of inhibitory cholinergic synaptic strength from the brainstem to the thalamus can change the rhythm of neural oscillation in the BTC

model significantly. It can induce not only a diminished dominant frequency but also a slowing of rhythmic content, i.e., a decreased alpha band activity and an increased theta band activity. These simulated phenomena as a result of acetylcholine deficiency agree with the EEG characteristics observed in the electrophysiological experiments of AD patients, i.e., the major effect of AD on EEG is slowing of EEG [18 19 20 21 22] along with the degraded peak frequency [15 16 17].

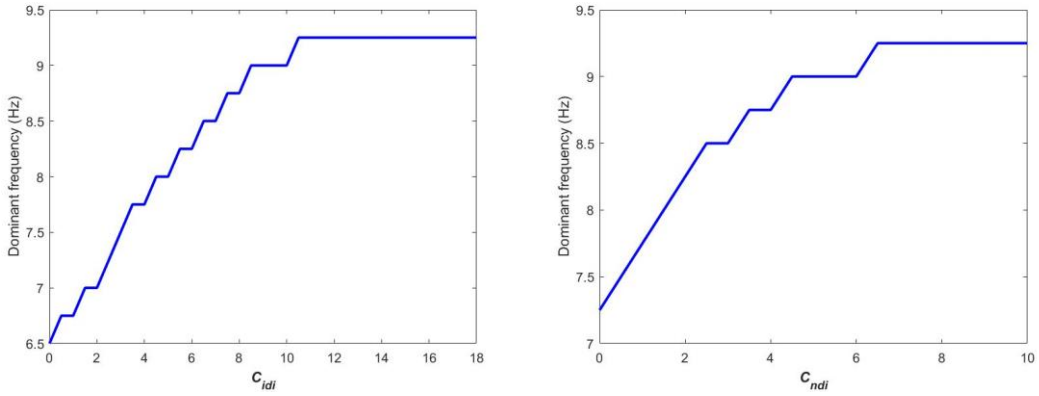

Fig 7 Dependence of the dominant frequency of the BTC model on the inhibitory cholinergic synapse connectivity C_{idi} from PNN to IN (left panel) and C_{ndi} from PNN to TRN (right panel).

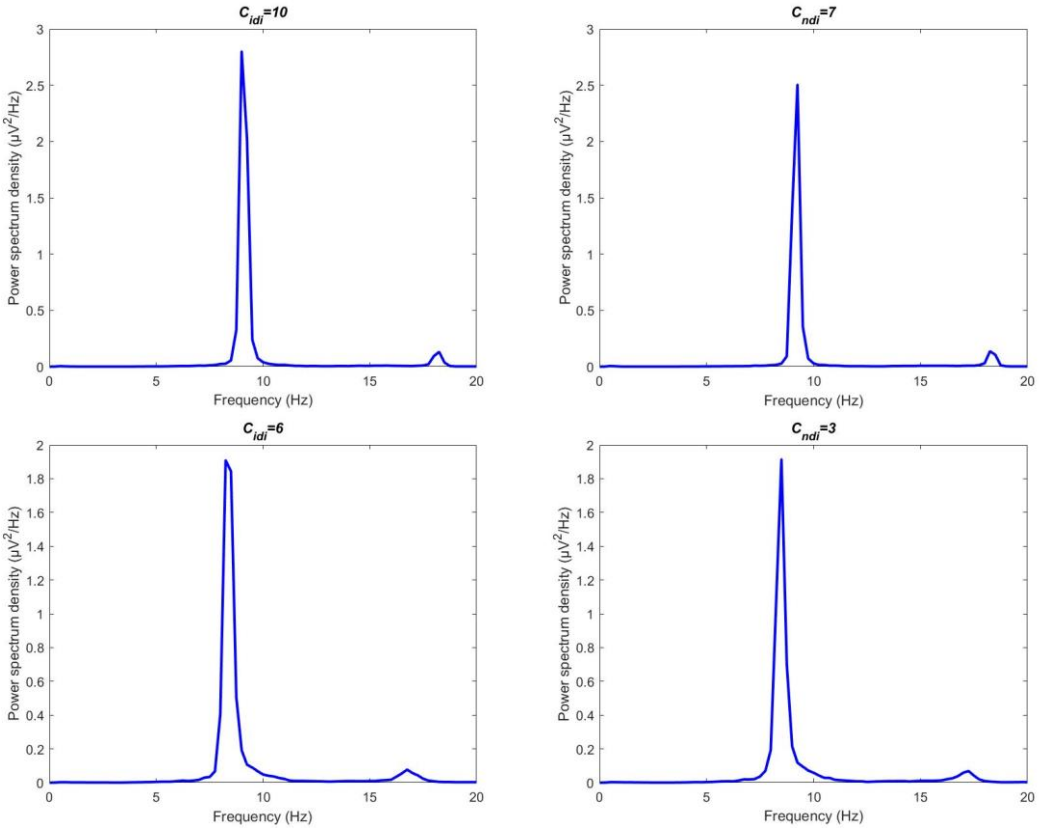

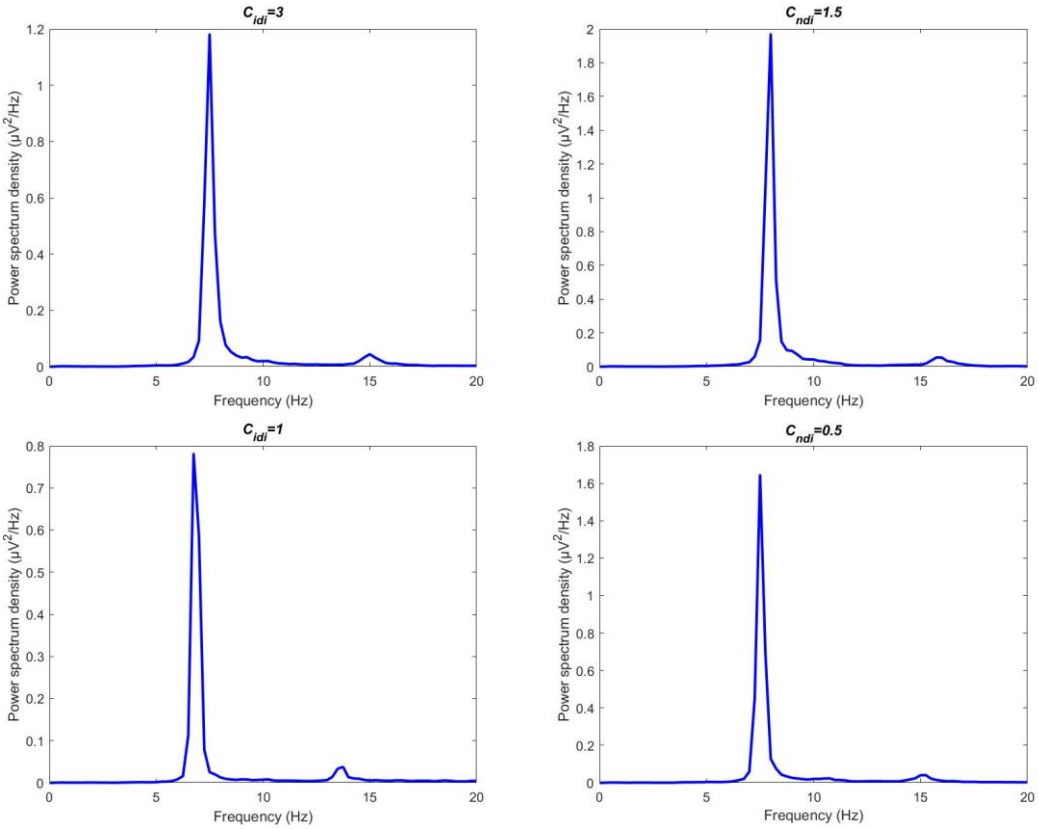

Fig 8 The individual plots of power spectrum density when the inhibitory cholinergic synapse connectivity takes different values. In left column, C_{idi} is taken as 10, 6, 3 and 1 from top to bottom. In right column, C_{ndi} is taken as 7, 3, 1.5 and 0.5 from top to bottom.

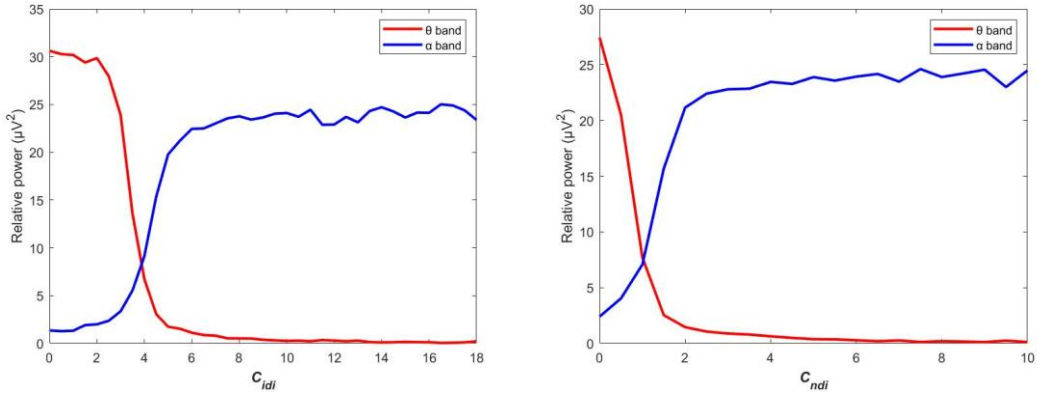

Fig 9 The evolution of relative power in alpha and theta frequency bands during the reduction of inhibitory cholinergic synapse connectivity. Left panel: the connectivity parameter C_{idi} (from PNN to IN) is varied in the range of [0,18]. Right panel: the connectivity parameter C_{ndi} (from PNN to TRN) is varied in the range of [0,10].

Secondly, the neural oscillation of the BTC model is explored in time-domain by analyzing oscillation amplitude of model output. **Fig 10** depicts the variation of the summated postsynaptic potential V_{trc} during [20, 120] s of simulations as the inhibitory cholinergic synapse connectivity is diminished. These two figures indicate that the oscillation amplitude is degraded as a whole upon diminishing the connectivity parameter C_{idi} or C_{ndi}, though this downward trend is not very smooth. In order to confirm this phenomenon, amplitude distribution at some synaptic strengths is further displayed in **Fig 11** according to the statistical property of 500 realizations of postsynaptic potential V_{trc}. From the fitted normal density function of oscillation amplitude, the left panels in Fig.11 reveal that the estimated mean of oscillation amplitude is successively 9.58, 8.66, 6.92 and 5.41 when C_{idi} = 10, 6, 3 and 1. On the same time, the right panels in **Fig 11** reveal that the estimated mean of oscillation amplitude decreases from 9.83 to 8.82, then to 7.76, and finally to 6.89 when C_{ndi} decreases from 7 to 3, then to 1.5, and finally to 0.5. These results imply that decrease in inhibitory cholinergic synapse connectivity from brainstem to thalamus resulting from acetylcholine deficit can indeed bring about a decrease in oscillation amplitude of the model output.

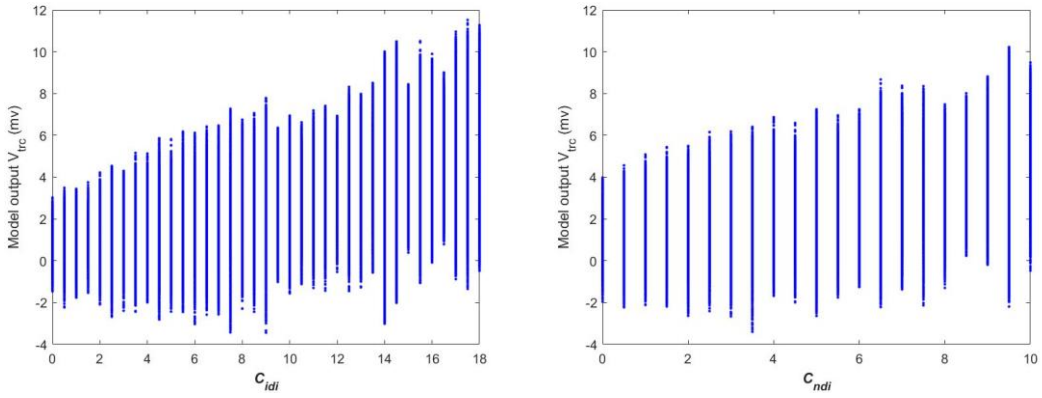

Fig 10 The model output of the summated postsynaptic potential V_{trc} for each inhibitory cholinergic synapse connectivity. Left panel: the connectivity parameter C_{idi} (from PNN to IN) is in the range of [0,18]. Right panel: the connectivity parameter C_{ndi} (from PNN to IN) is in the range of [0,10].

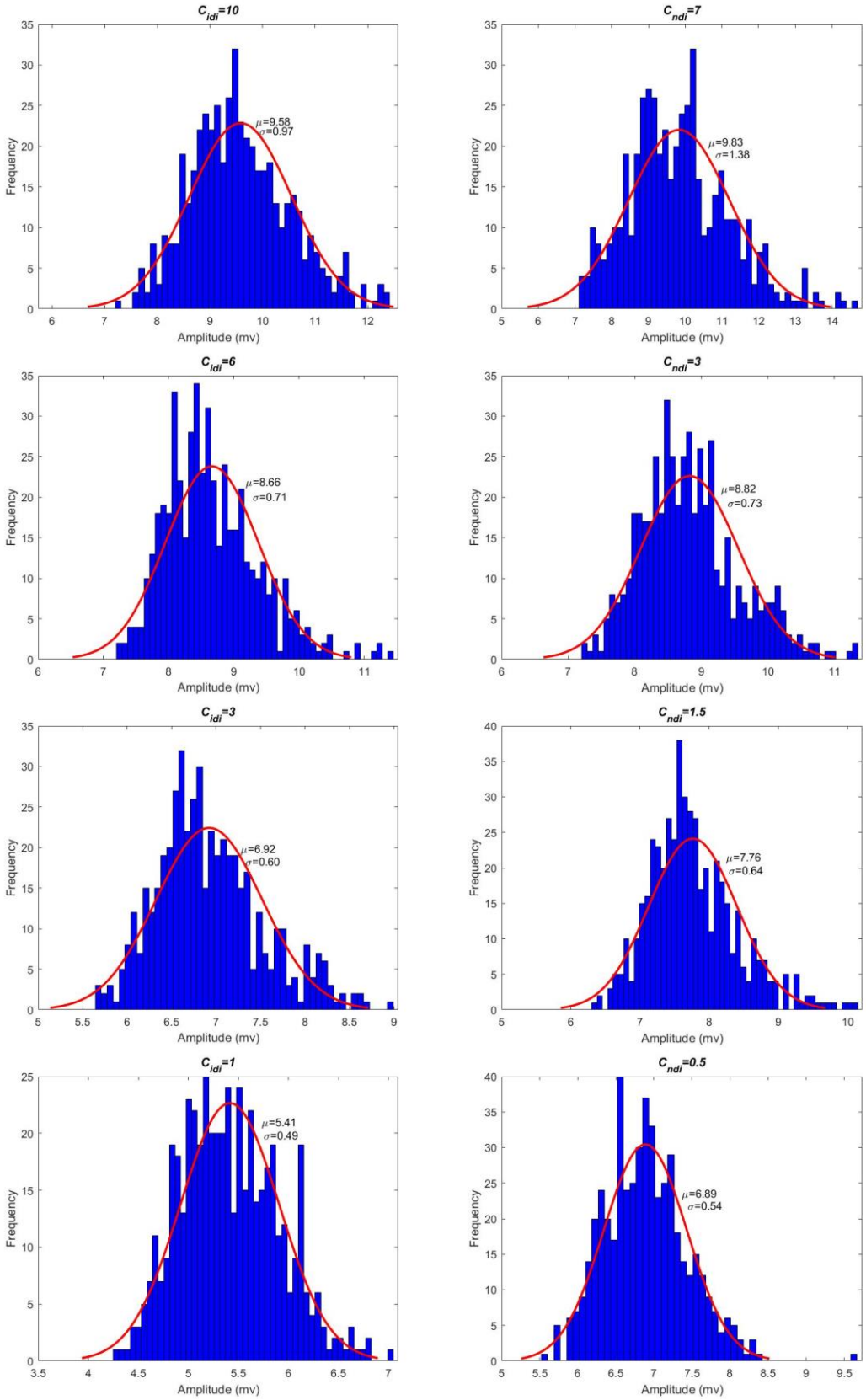

Fig 11 The amplitude distribution of V_{trc} for some different inhibitory connectivity parameter values. Left column: the connectivity parameter C_{idi} is in turn 10, 6, 3 and

1 from top to bottom. Right column: the connectivity parameter C_{ndi} is in turn 7, 3, 1.5 and 0.5 from top to bottom.

3.3 Decreasing the excitatory glutamatergic connectivity from PY to PNN

As illustrated by the schematic of BTC model in **Fig 1**, the release of acetylcholine from brainstem to thalamus is indirectly modulated by glutamatergic synapse pathway from cortex to brainstem. The synapse loss caused by cortical atrophy in AD may destroy the descending synapse projection from cortex to brainstem [44 45]. In this section, decreasing the glutamatergic synapse connectivity C_{dpe} from PY in cortex to PNN in brainstem to mimic indirect acetylcholine deficiency, neural oscillation in this BTC model is discussed using power spectrum analysis and oscillation amplitude.

Firstly, the property of neural oscillation is characterized by the dominant frequency and the relative power in frequency-domain. The evolution of dominant frequency of the model output V_{trc} during the decrease of C_{dpe} is depicted in **Fig 12**. Clearly, as C_{dpe} is diminished from 78 to 38, the dominant frequency initially falls within alpha frequency band until C_{dpe} arrives at a critical value of 45, and then the dominant frequency continues to fall within theta frequency band with a further decrease of C_{dpe}. Individual curves of power spectrum density at some synaptic strength are further given in **Fig 13** to confirm the above phenomenon. As shown in the upper two panels(C_{dpe}=65, 48), the peak value of power spectrum density is obtained at about 9.25 and 8.5, i.e., the dominant frequency is located within alpha frequency band when the synaptic connectivity is large than the critical value of 45. Nevertheless, as displayed in the lower two panels (C_{dpe}=41, 38), the dominant frequency is respectively 7 and 6.5, which indicates the peak of power spectrum density is located within theta frequency band when the synaptic connectivity is smaller than the critical value of 45. Furthermore, the variation of relative power along with the synaptic connectivity C_{dpe} is displayed in **Fig 14.** Upon decreasing C_{dpe} from 78, the relative alpha band power in the left panel fluctuates slightly until C_{dpe} reaches a certain value of 45, then it falls sharply till $C_{dpe} \approx 38$. Interestingly, an

opposite situation occurs with respect to the relative theta band power in the right panel, i.e., the relative power within theta band rises slightly until C_{dpe} arrives at the certain value of 45, then it booms quickly till $C_{dpe} \approx 38$. As we expected, the rhythmic property of neural oscillation in this BTC model resulting from glutamatergic synapse deficit is similar with that what happened in the case of direct acetylcholine deficiency, i.e., the diminished dominant frequency, the degraded alpha band activity together with enhanced theta band activity, which is consistent with the EEG characteristic obtained from clinical trials of AD patients [15 17 20 22].

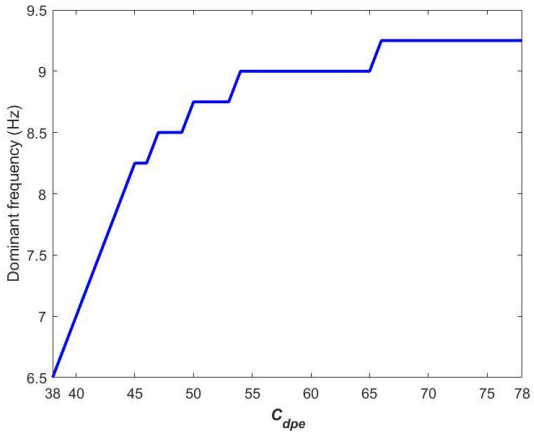

Fig 12 Dependence of the dominant frequency of the BTC model output on the excitatory glutamatergic synapse connectivity C_{dpe} from PY to PNN.

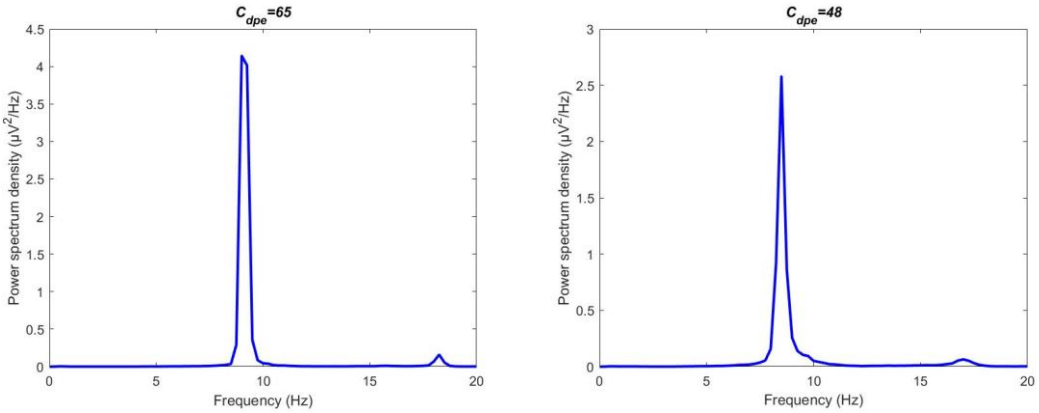

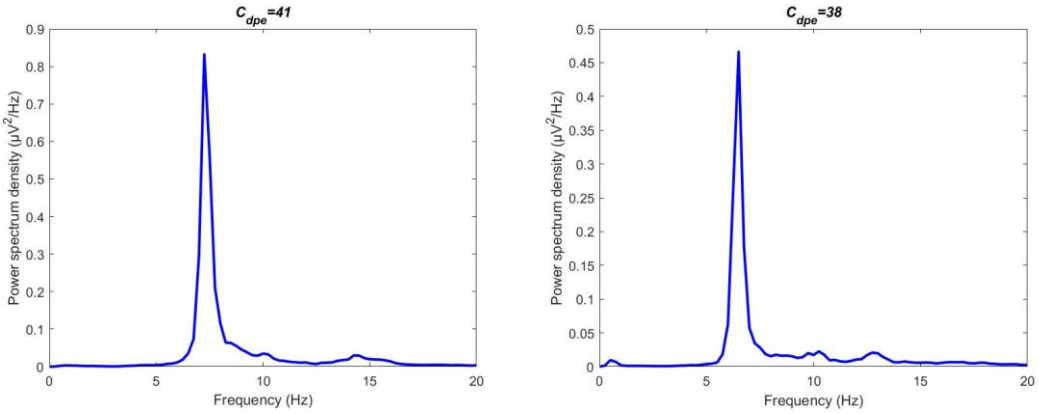

Fig 13 Single curves of the power spectrum density when the excitatory glutamatergic synapse connectivity parameter C_{dpe} takes some different values of 65, 48, 41 and 38.

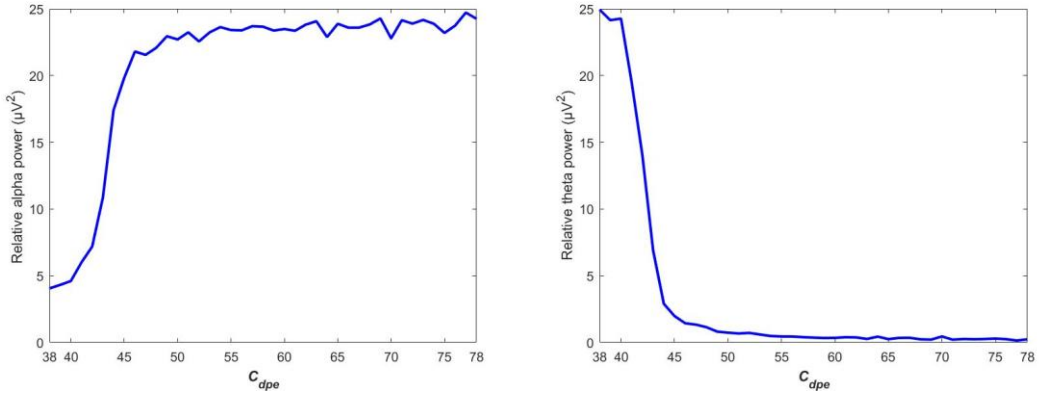

Fig 14 The evolution of relative power in specific frequency bands during the excitatory synapse connectivity parameter C_{dpe} is varied in the range of [38,78]: (left panel) the relative power within alpha band, (right panel) the relative power within theta band.

Secondly, neural oscillation of model output in the BTC model is studied by means of oscillation amplitude in time-domain. **Fig 15** depicts the summated postsynaptic potential V_{trc} of model output during [20, 120] s of simulations for every connectivity parameter C_{dpe} ranged in [38,78]. Intuitively, as C_{dpe} is decreased from 78 to 38 the oscillation amplitude of V_{trc} slowly descends as a whole except for few connectivity strength at which the oscillation amplitude is suddenly enlarged. In addition, this result is visualized in **Fig 16** by some individual postsynaptic potential V_{trc} at different synaptic strength such as C_{dpe} = 38, 41, 48, and 65. Combined with the dominant frequency shown in **Fig 12**, the upper two panels in the left column reveal that the postsynaptic potential has an visible alpha rhythmic content with the

amplitude waxing and waning when the synapse connectivity is greater than the critical value of 45. Whereas, in the lower two panels there appears an obvious theta rhythmic content in the postsynaptic potential with relatively small oscillation amplitude when the synapse connectivity is less than the critical value of 45. Furthermore, the corresponding amplitude distribution of 500 realizations of postsynaptic potential is illustrated in the right column of **Fig 16**. One can observe that the estimated mean of oscillation amplitude is in turn 9.63, 8.96, 6.57 and 4.83 on the basis of the fitted normal density function of oscillation amplitude. This quantitative result once again confirms that the decreased oscillation amplitude of model output is due to the damaged glutamatergic synapse connectivity C_{dpe} from PY to PNN, an indirect acetylcholine synapse pathway from cortex to brainstem.

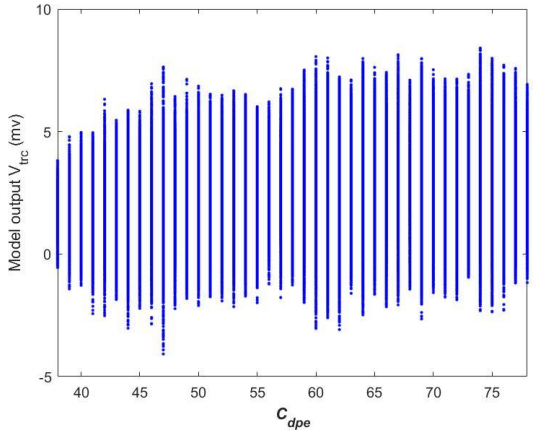

Fig 15 The model output of the summated postsynaptic potential V_{trc} for each excitatory synapse connectivity parameter C_{dpe} in the range of [38,78].

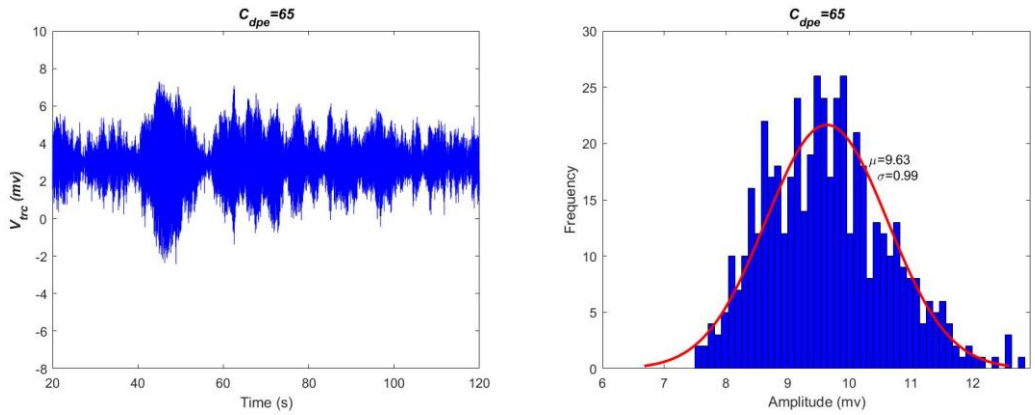

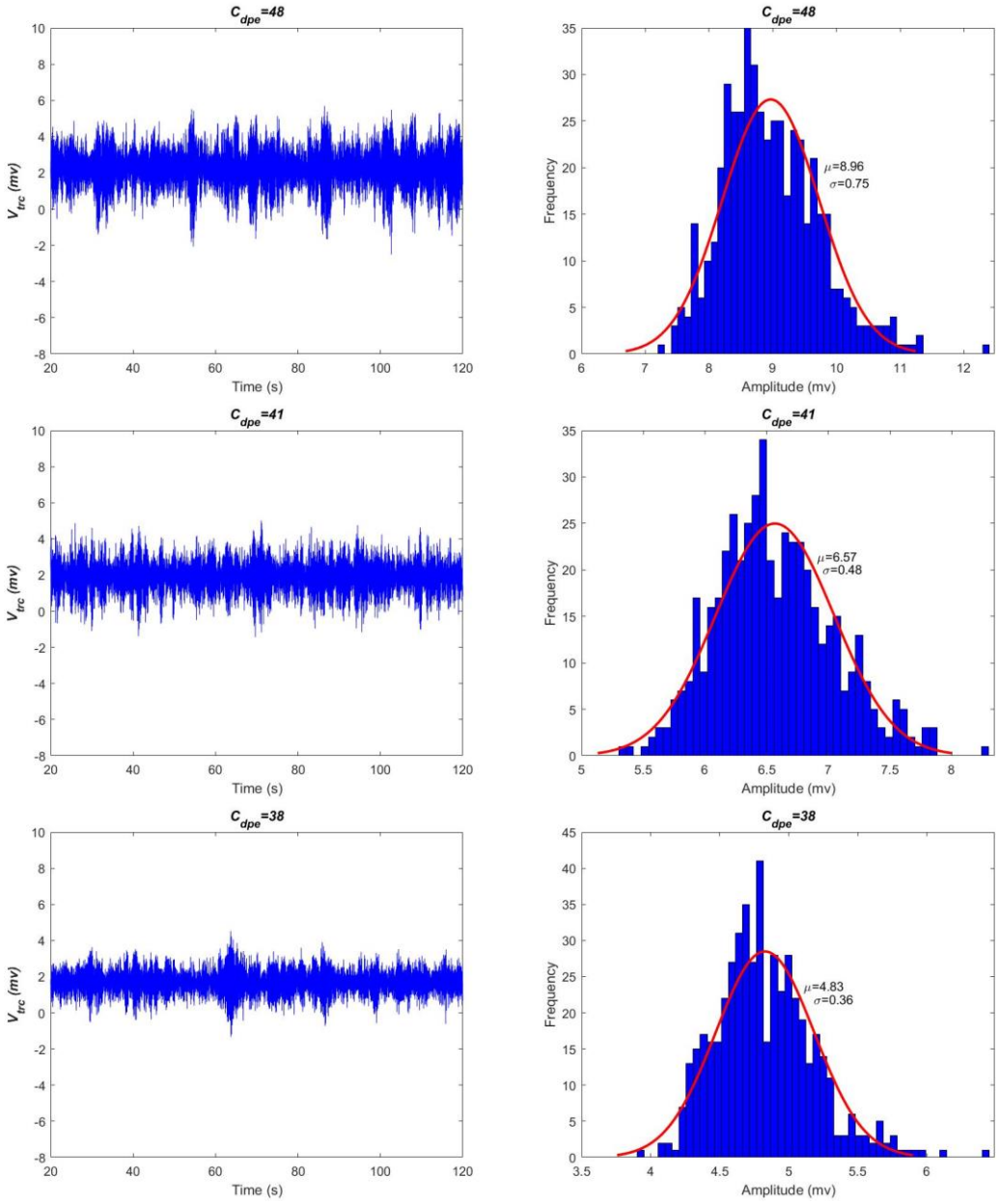

Fig 16 Plots of the summated postsynaptic potential V_{trc} (left column) and the corresponding amplitude distribution of V_{trc} (right column) for some different connectivity parameter values. From top to bottom, the connectivity parameter C_{dpe} is in turn 65, 48, 41 and 38.

Conclusion and discussion

This work establishes a comprehensive neural mass model in the interactive brain structures of brainstem, thalamus and cortex. It takes destroying cholinergic synapse pathway as a surrogate for the abnormal cholinergic system in patients with AD. By monitoring synapse connectivity strength in direct cholinergic pathway from

brainstem to thalamus and indirect glutamatergic synapse pathway from cortex to brainstem, we are able to simulate some property of neural oscillation in this model under an environment of acetylcholine deficiency from the standpoint of neurocomputation. By analyzing power spectrum of the model output in frequency domain, the results reveal that upon diminishing synapse connectivity strength in a certain range the dominant frequency initially decreases within alpha frequency band and then steps into theta frequency band. Meanwhile, the neural oscillation presents a slowing rhythmic content with a degraded alpha band relative power and an enhanced theta band relative power. What's more, amplitude distribution of the neural oscillation in time domain suggests that the oscillation amplitude is as a whole diminished with the reduction of synapse connectivity. Our results accord with the electrophysiological EEG characteristics reported in clinical experiments of AD patients. We expect these findings could have important implications on better understanding cholinergic pathogenesis and expounding potential feature for AD.

At last, we point out that this work, by reducing the synaptic connection parameters in cholinergic direct pathway from brainstem to thalamus or indirect glutamatergic synapse pathway from cortex to brainstem, mainly focus on the effect of acetylcholine deficiency on brain neuron activity in patients with AD. As known that there could be neuron loss and brain atrophy in cortical region in AD patients [44 45], which would induce unfavorable synapse information processing. Thus, reducing the synaptic connection parameters relative to cortical region can also simulate the pathological state of AD. Through further simulation, we find that when decreasing synapse connectivity parameter from PY to TRC the change of the dominant frequency and the oscillation amplitude is similar with what reported in this work, i. e. there is an obvious decrease of dominant frequency, a degraded rhythmic activity in alpha frequency band as well as an enhanced rhythmic activity in theta frequency band, and the reduced oscillation amplitude of the model output. For the limited space, we do not list them in detail.

Acknowledgments

This work is partially supported by the National Natural Science Foundation of China (Grant No. 11972217), the Fundamental Funds Research for the Central Universites (Grant Nos. GK201901008).

Authors Contributions

Hao Yang and XiaoLi Yang contributed to the conception of this work, designed

research, analyzed data and wrote the main manuscript text. SiLu Yan and ZhongKui Sun performed the analysis and proposed constructive advice. All authors reviewed the manuscript.

Declarations

We declare that we have no potential conflict of interest.

Availability of Data and Materials

All data generated or analysed during this study are included in this published article.

References

[1] Zatorre, R. J., Fields, R. D. & Johansen-Berg, H. Plasticity in gray and white: neuroimaging changes in brain structure during learning. *Nat. Neuroscienc*, **15**(4), 528-536 (2012).

[2] Geula, C. Abnormalities of neural circuitry in Alzheimer’ s disease: hippocampus and cortical cholinergic innervation. *Neurology*, **51**(Suppl 1), S18-S29 (1998).

[3] Hasselmo, M. E. The role of acetylcholine in learning and memory. *Curr. Opin. Neurobiol.* **16**, 710-715 (2006).

[4] Sarter, M., Hasselmo, M. E., Bruno, J. P. & Givens, B. Unraveling the attentional functions of cortical cholinergic inputs: interactions between signal-driven and cognitive modulation of signal detection. *Brain Res. Rev.* **48**, 98-111 (2005).

[5] Auld, D. S., Kornecook, T. J., Bastianetto, S. & Quirion, R. Alzheimer's disease and the basal forebrain cholinergic system: relations to beta-amyloid peptides, cognition, and treatment strategies. *Prog Neurobiol.* **68**, 209-245 (2002).

[6] Nilsson, L., Nordberg, A., Hardy, J., Wester, P. & Winblad, B. Physostigmine restores 3H-acetylcholine efflux from Alzheimer brain slices to normal level. *J. Neural Transm.* **67**, 275-285 (1986).

[7] Lopez, O. L. et al. Severity of cognitive impairment and the clinical diagnosis of AD with Lewy bodies. *Neurology*, **54**, 1780-1787 (2000).

[8] Oda, Y. Choline acetyltransferase: the structure, distribution and pathologic changes in the central nervous system. Pathol. Int. **49**, 921-937 (1999) .

[9] McCormick, D. A. & Pape, H. C. Acetylcholine inhibits identified interneurons in the cat lateral geniculate nucleus. Nature. **334**, 246-248 (1988).

[10] Mesulam, M. M. Cholinergic pathways and the ascending reticular activating system of the human brain. *Ann. NY. Acad. Sci*. **757**, 169-179 (1995).

[11] Billet, S., Cant, N. B. & Hall, W. C. Cholinergic projections to the visual thalamus and superior colliculus. *Brain Res*. **847**, 121-123 (1999).

[12] Koyama, Y., Jodo, E. & Kayama, Y. Sensory responsiveness of “Broad-spike” neurons in the laterodorsal tegmental nucleus, locus coeruleus and dorsal raphe of awake rats: Implications for cholinergic and monoaminergic neuron-specific responses. *Neuroscience*, **63**, 1021-1031 (1994).

[13] Brown, R. E., Basheer, R., Mckenna, J. T., Strecker, R. E. & McCarley R. W. Control of Sleep and Wakefulness. *Physiol. Rev.* **92**, 1087-1187 (2012)

[14] Parvizi, J., Hoesen, G. W. V. & Damasio, A. The selective vulnerability of brainstem nuclei to Alzheimer's disease. *Ann. Neurol.* **49**, 53-66 (2001).

[15] Prinz, P. N. & Vitiell, M. V. Dominant occipital (alpha) rhythm frequency in early stage Alzheimer's disease and depression. *Electroencephalogr. Clin. Neurophysiol.* **73**, 427-432 (1989).

[16] Penttilä, M., Partanen, J. V., Soininen, H. & Riekkinen, P. J. Quantitative analysis of occipital EEG in different stages of Alzheimer's disease. *Electroencephalogr. Clin. Neurophysiol.* **60**, 1-6 (1985).

[17] Moretti, D. V. et al. Individual analysis of EEG frequency and band power in mild Alzheimer's disease. *Clin. Neurophysiol.* **115**, 299-308 (2004).

[18] Dauwels, J., Vialatte, F. & Cichocki, A. Diagnosis of Alzheimer’s disease from EEG signals: where are we standing. *Curr. Alzheimer. Res.* **7**, 487-505 (2010).

[19] Coben, L. A., Danziger, W. & Storandt, M. A longitudinal EEG study of mild senile dementia of Alzheimer type: changes at 1 year and at 2.5 years. *J. Electroencephalogr. Clin. Neurophysiol.* **60**, 1-6 (1985).

[20] Jeong, J. EEG dynamics in patients with Alzheimer’s Disease. *Neurophysiology*, **115**, 1490-1505 (2004).

[21] Besthorn, C. Discrimination of Alzheimer's disease and normal aging by EEG data. *J. Electroencephalogr. Clin. Neurophysiol.* **103**, 241-248 (1997).

[22] Ebert, U., Crossmann, M., Oertel, R., Gramatte, T. & Kirch, T. Pharmacokinetic-Pharmacodynamic Modeling of the Electroencephalogram Effects of Scopolamine in Healthy Volunteers. *J. Clin. Pharmacol.* **41**, 51-60 (2001).

[23] Jiang, P. H., Yang, X. L. & Sun, Z. K. Dynamics analysis of the hippocampal neuronal model subjected to cholinergic action related with Alzheimer's disease. *Cogn. Neurodynamics*, **14**(1) (2020).

[24] Hassan, M. et al. Computational modeling and biomarker studies of pharmacological treatment of Alzheimer's disease (Review). *Mol. Med. Rep*. **18**, 639-655 (2018).

[25] Breakspear, M. Dynamic models of large-scale brain activity. *Nat. Neurosci.* **20**, 340-352 (2017).

[26] Li, X. Y., Yang, X. L. & Sun, Z. K. Alpha rhythm slowing in a modified thalamo-cortico-thalamic model related with Alzheimer's disease. *PLoS One*, **15**, e0229950 (2020).

[27] David, O. Neural Mass Models. *Brain Mapping*, **1**, 563-569 (2015).

[28] Zavaglia, M., Astolfi, L., Babiloni, F. & Ursino, M. A neural mass model for the simulation of cortical activity estimated from high resolution EEG during cognitive or motor tasks. *J. Neurosci. Methods*, **157**, 317-329 (2006).

[29] Ursino, M., Cona, F. & Zavaglia, M. The generation of rhythms within a cortical region: Analysis of a neural mass model. *J. Neuroimage*, **52**, 1080-1094 (2010).

[30] Wilson, H. R. & Cowan, J. D. Excitatory and inhibitory interaction in localized populations of model neurons. *Biophys. J.* **12**, 1-24 (1972).

[31] Wilson, H. R. & Cowan, J. D. A mathematical theory of the functional dynamics of cortical and thalamic nervous tissue. *Kybernetik*, **13**, 55-80 (1973).

[32] Silva, F. H. L. D., Hoeks, A., Smits, H. & Zetterberg, L. H. Model of brain rhythmic activity. The alpha-rhythm of the thalamus. *Kybernetik*, **15**, 27-37 (1974).

[33] Jansen, B. H. & Rit, V. G. Electroencephalogram and visual evoked potential generation in a mathematical model of coupled cortical columns. *Biol. Cybern.* **73**, 357-366 (1995).

[34] Wendling, F., Bartolomei, F., Bellanger, J. J. & Chauvel, P. Epileptic fast activity can be explained by a model of impaired GABAergic dendritic inhibition. *Eur. J. Neurosci.* **15**, 1499-1508 (2002).

[35] Deco, G., Jirsa, V. K., Robinson, P. A., Breakspear, M. & Firstonk, K. The Dynamic Brain: From Spiking Neurons to Neural Masses and Cortical Fields. *PLoS Comput. Biol.* **4**, e1000092 (2008).

[36] Spiegler, A., Kiebel, S. J., Atay, F. M. & Knösche, T. R. Bifurcation analysis of neural mass models: Impact of extrinsic inputs and dendritic time constants. *Neuroimage*, **52**, 1041-1058 (2010).

[37] Bhattacharya, B. S., Coyle, D. & Maguire, L. P. A thalamo-cortico-thalamic neural mass model to study alpha rhythms in Alzheimer's disease. *Neural. Netw.* **24**, 631-645 (2011).

[38] Guillery, R. W. & Sherman, S. M. Thalamic relay functions and their role in corticocortical communication: generalizations from the visual system. *Neuron*,

33, 163-175 (2002).

[39] McCormick, D. A. & Bal, T. Sleep and arousal: thalamocortical mechanisms. *Annu. Rev. Neurosci.* **20**, 185-215 (1997).

[40] Kolmac, C. I. & Mitrofanis, J. Patterns of brainstem projection to the thalamic reticular nucleus. *J. Comp. Neurol.* **396**, 531-543 (1998).

[41] Jeon, C. J., Gurski, M. R. & Mize, R. R. Glutamate containing neurons in the cat superior colliculus revealed by immunocytochemistry. *Visual Neurosci.* **14**, 387-393 (1997).

[42] Beatty, J. A., Sylwestrak, E. L. & Cox, C. L. Two distinct populations of projection neurons in the rat lateral parafascicular thalamic nucleus and their cholinergic responsiveness. *Neuroscience*, **162**, 155-173 (2009).

[43] Plummer, K. L., Manning, K. A., Levey, A. I., Ress, H. D. & Uhlkich, D J. Muscarinic receptor subtypes in the lateral geniculate nucleus: A light and electron microscopic analysis. *J. Comp. Neurol.* **404**, 408-425 (1999).

[44] Matsumura, M. et al. Organization of somatic motor inputs from the frontal lobe to the pedunculopontine tegmental nucleus in the macaque monkey. *Neuroscience*, **98**, 97-110 (2000).

[45] Wallace, M. T., Meredith, M. A. & Stein, B. E. Converging influences from visual, auditory, and somatosensory cortices onto output neurons of the superior colliculus. *J. Neurophysiol.* **69**, 1797-1809 (1993).

[46] Erisir, A., Horn, S. C. V. & Sherman, S. M. Distribution of synapses in the lateral geniculate nucleus of the cat: Differences between laminae A and A1 and between relay cells and interneurons. *J. Comp. Neurol.* **390**, 247-255 (1998).

[47] Erisir, A., Horn, S. C. V. & Sherman, S. M. Relative numbers of cortical and brainstem inputs to the lateral geniculatenucleus. *Proc. Natl. Acad. Sci. U. S. A.* **94**, 1517-1520 (1997).

[48] Jones, E. G. Thalamic circuitry and thalamocortical synchrony. *Philos. Trans. R. Soc. B-Biol. Sci.* **357**, 1659-1673 (2002).

[49] Liu, X. B. & Jones, E. G. Predominance of Corticothalamic Synaptic Inputs to Thalamic Reticular Nucleus Neurons in the Rat. *J. Comp. Neurol.* **414**, 67-79 (1999).

[50] Haith, G. L. Modeling Activity-Dependent Development in the Retinogeniculate Projection. *Stanford University* (1998).

[51] Sotero, R. C., Barreto, N. G. T., Medina, Y. I., Carbonell F. & Jimenez J. C. Realistically Coupled Neural Mass Models Can Generate EEG Rhythms. *Neural*

Comput. **19**, 478-512 (2007).

[52] Braak, H. & Braak, E. Neuropathological stageing of Alzheimer-related changes. *Acta. Neuropathol.* **82**, 239-259 (1991).

[53] Seeley, W. W., Crawford, R. K., Zhou, J., Miller B. C. & Greicius, M. D. Neurodegenerative diseases target large-scale human brain networks. *Neuron*, **62**, 42-52 (2009).